



Drug Screening Identifies Sigma-1-Receptor as a Target for the Therapy of VWM Leukodystrophy

Andrea Atzmon¹, Melisa Herrero¹, Reut Sharet-Eshed¹, Yocheved Gilad², Hanoch Senderowitz² and Orna Elroy-Stein^{1,3*}

¹ The School for Molecular Cell Biology and Biotechnology, George S. Wise Faculty of Life Sciences, Tel Aviv University, Tel Aviv, Israel, ² Department of Chemistry, Bar-Ilan University, Ramat-Gan, Israel, ³ Sagol School of Neuroscience, Tel Aviv University, Tel Aviv, Israel

OPEN ACCESS

Edited by:

Hermona Soreq,
The Hebrew University of Jerusalem,
Israel

Reviewed by:

Graham D. Pavitt,
The University of Manchester,
United Kingdom
Tsung-Ping Su,
National Institutes of Health (NIH),
United States

*Correspondence:

Orna Elroy-Stein
omaes@tauex.tau.ac.il

Received: 18 May 2018

Accepted: 27 August 2018

Published: 18 September 2018

Citation:

Atzmon A, Herrero M, Sharet-Eshed R, Gilad Y, Senderowitz H and Elroy-Stein O (2018) Drug Screening Identifies Sigma-1-Receptor as a Target for the Therapy of VWM Leukodystrophy.

Front. Mol. Neurosci. 11:336.
doi: 10.3389/fnmol.2018.00336

Vanishing white matter (VWM) disease is an autosomal genetic leukodystrophy caused by mutations in subunits of eukaryotic translation initiation factor 2B (eIF2B). The clinical symptoms exhibit progressive loss of white matter in both hemispheres of the brain, accompanied by motor functions deterioration, neurological deficits, and early death. To date there is no treatment for VWM disease. The aim of this work was to expedite rational development of a therapeutic opportunity. Our approach was to design a computer-aided strategy for an efficient and reliable screening of drug-like molecules; and to use primary cultures of fibroblasts isolated from the Eif2b5^{R132H/R132H} VWM mouse model for screening. The abnormal mitochondria content phenotype of the mutant cells was chosen as a read-out for a simple cell-based fluorescent assay to assess the effect of the tested compounds. We obtained a hit rate of 0.04% (20 hits out of 50,000 compounds from the selected library). All primary hits decreased mitochondria content and brought it closer to WT levels. Structural similarities between our primary hits and other compounds with known targets allowed the identification of three putative cellular pathways/targets: 11 β -hydroxysteroid dehydrogenase type 1, Sonic hedgehog (Shh), and Sigma-1-Receptor (S1R). In addition to initial experimental indication of Shh pathway impairment in VWM mouse brains, the current study provides evidence that S1R is a relevant target for pharmaceutical intervention for potential treatment of the disease. Specifically, we found lower expression level of S1R protein in fibroblasts, astrocytes, and whole brains isolated from Eif2b5^{R132H/R132H} compared to WT mice, and confirmed that one of the hits is a direct binder of S1R, acting as agonist. Furthermore, we provide evidence that treatment of mutant mouse fibroblasts and astrocytes with various S1R agonists corrects the functional impairments of their mitochondria and prevents their need to increase their mitochondria content for compensation purposes. Moreover, S1R activation enhances the survival rate of mutant cells under ER stress conditions, bringing it to WT levels. This study marks S1R as a target for drug development toward treatment of VWM disease. Moreover, it further establishes the important connection between white matter well-being and S1R-mediated proper mitochondria/ER function.

Keywords: leukodystrophy, drug screening, vanishing white matter (VWM), mitochondria dysfunction, eIF2B, Sigma-1-Receptor (S1R), agonist, drug-like compounds

INTRODUCTION

Vanishing white matter (VWM) disease, also termed Childhood ataxia with CNS hypomyelination (CACH), is a genetic autosomal recessive leukodystrophy characterized by progressive loss of white matter in both hemispheres of the brain. The consequent axonal degeneration results in progressive impairments of neurologic functions, leading to complete paralysis and early death (Schiffmann and Elroy-Stein, 2006; Elroy-Stein and Schiffmann, 2015). Disease onset and clinical symptoms refer to congenital, classical, and adult forms. The congenital form is extremely rare; the classical form refers to disease onset at early childhood and death around late teens, with <1000 known patients in the world; the adult form which seems increasingly common refers to a mild version of clinical symptoms and their slow progression. An important feature of all forms of this genetic orphan disease is the deterioration of clinical symptoms upon exposure to physiological and environmental stressors (Fogli and Boespflug-Tanguy, 2006).

Vanishing white matter disease is caused by partial-loss-of-function mutations in any of the five genes encoding the subunits of eIF2B (Leegwater et al., 2001). eIF2B is a master regulator of mRNA translation at the hub of the integrated stress response (ISR) (Pavitt, 2018). The five subunits of eIF2B, which assemble into a decameric $(\alpha\beta\delta\gamma\epsilon)_2$ complex (Kashiwagi et al., 2016), recycle GDP-bound eIF2 back to its active GTP-bound form, under normal conditions, while it fails to do so when eIF2 α is phosphorylated upon stress. Hypo-active eIF2B renders mutant cells hyper-sensitive to endoplasmic reticulum (ER) stress (Kantor et al., 2005).

To further study the disease etiology, we have previously developed the Eif2b5^{R132H/R132H} mouse strain which is homozygous for one of the VWM mutations. This mouse model exhibits ~20% decrease in eIF2B enzymatic activity in the brain, which is associated with white matter deficits and mild impairment of motor functions. Eif2b5^{R132H/R132H} mice provided fundamental insights related to the effect of eIF2B mutations, including delayed postnatal brain development, failure to overcome cuprizone-induced demyelination, abnormal glial cell abundance, increased abundance of demyelinated axons, and axons ensheathed with split and damaged myelin (Geva et al., 2010). Astrocytes are considered central in the patho-mechanism of the disease (Dooves et al., 2016), yet eIF2B mutations lead to cellular phenotype impairments also in microglia, associated with poor cerebral inflammatory response upon insults (Cabilly et al., 2012). At the molecular level, we have demonstrated delayed waves of gene expression, unbalanced expression of unfolded proteins response (UPR)-related genes, impaired oxidative respiration, and increased mitochondrial content to compensate for energetic requirements (Marom et al., 2011; Gat-Viks et al., 2015; Raini et al., 2017).

To date there is no treatment for VWM disease. Earlier attempts to identify eIF2/eIF2B modifying compounds in the context of ISR or eIF2B mutations involved a recombinant yeast-based assay for high-throughput screening (Motlekar et al., 2009). A later use of recombinant stress-reporting assay in mammalian

cells identified a molecule, known as ISRIB (Sidrauski et al., 2013). ISRIB stabilizes the decameric form of eIF2B and restores the residual catalytic activity of some eIF2B mutant complexes to wild-type (WT) levels, while rendering it insensitive to the inhibitory effect of eIF2 α phosphorylation (Wong et al., 2018; Zyryanova et al., 2018). In the current study, we undertook a different approach by using the defective mitochondrial phenotype of primary fibroblasts isolated from Eif2b5^{R132H/R132H} mice. We used this cellular phenotype to develop a cellular assay for screening of compounds that decrease mitochondria content. By comparing the structure of 19 relevant hits to that of compounds with known biological targets, 6 were mapped to three putative cellular targets/pathways: Sonic hedgehog (Shh), Sigma-1-Receptor (S1R), and 11 β -hydroxysteroid dehydrogenase type 1 (11 β -HSD1). We experimentally confirmed that four compounds act as antagonists/agonists of the Shh signaling pathway and provided an initial indication that it is impaired in VWM disease. Moreover, we demonstrated lower expression level of S1R protein in fibroblasts, astrocytes, and whole brains isolated from Eif2b5^{R132H/R132H} mice. Importantly, the current study clearly shows that treatment of mutant MEFs and astrocytes with S1R agonists corrects their mitochondrial functional impairments and enhances their survival rate under ER-stress conditions. Therefore, this study marks S1R as a highly relevant target for pharmacological intervention for the treatment of VWM disease.

MATERIALS AND METHODS

Mice and Cells

Wild-type (C57BL strain) and Eif2b5^{R132H/R132H} (Mut; mutant) mice of both sexes were bred and housed in Tel Aviv University animal facility with 14/10 h light/dark cycle in groups of four animals per cage in individually ventilated cages (Lab Products Inc., Seaford, DE, United States) supplemented with autoclaved wood chips. Animals fed with autoclaved rodent pellet (Koffolk 19-510; Koffolk Ltd., Petach Tikva, Israel) and sterile water *ad libitum*. All experimental procedures were approved by the Tel Aviv University Animal Care Committee according to national guidelines (permits #L-15-037 and #04-12-27). Breeding and genotyping was performed as previously described (Geva et al., 2010). Each generation was established by back cross of homozygous Mut with WT C57BL/6J (Harlan Labs, Jerusalem, Israel) to prevent genetic drift. Primary cultures of MEFs (from E14 embryos) and astrocytes (from P0-P2 newborns) were isolated and used as previously described (Raini et al., 2017).

Sonic hedgehog-light2 cells (Taipale et al., 2000) were maintained in DMEM supplemented with 10% fetal bovine serum, 100 U/ml penicillin, 0.1 mg/ml streptomycin, 2 mM L-glutamine, 400 μ g/ml G418 (A.G. Scientific), and 200 μ g/ml Zeocin (InvivoGen).

RNA and Protein Extractions From Brains

Brains were removed from p14, P18, and P21 mice. Cerebrums were flash frozen in liquid nitrogen and kept in -80°C until

use. RNA was extracted from left hemispheres using RiboEX (GeneAll). Proteins were extracted from left hemispheres by sonication in 500 μ l per hemisphere of lysis buffer containing 1% triton, 0.5% NaDOC, 0.1% SDS, 50 mM Tris pH 8, 100 mM NaCl, 10 mM β -glycerophosphate, 5 mM NaF, 1 mM DTT, 1 mM vanadate, and EDTA-free completeTM protease inhibitor cocktail (#11-836-170-001; ROCHE). After spinning for 15 min, 13,000 rpm, 4°C, the supernatant was analyzed for total concentration using BCA protein assay kit (#23227 Pierce).

Compounds

The compounds selected from DIVERSetTM-EXP library and H8 analogs were purchased from ChemBridge (San Diego, CA, United States). SAG (#4366), cyclopamine (#1623), pre-084 (#0589), and NE-100 (#3133) were from Tocris Bioscience. Pridopidine (#M326195) was from Toronto Research Chemicals (Toronto, ON, Canada), Tunicamycin (#T7765) from Sigma. All compounds were dissolved in DMSO, cyclopamine was dissolved in ethanol.

Selection and Clustering of Screening Library

The algorithm for the selection of optimal screening libraries is described in detail in Gilad et al. (2015) and was followed with no modifications. Each of the 50,000 compounds comprising the DIVERSetTM-EXP library was characterized by the ECFP6 fingerprints as implemented in BIOVIA's Discovery Studio Version 3.5 and clustered into 500 clusters using the Hierarchical clustering as implemented in Schrödinger's Canvas (Canvas, Schrödinger, LLC, New York, NY, 2018, United States). From each cluster, a compound closest to its center was selected for biological evaluation.

Docking and *in vitro* Confirmation of S1R Binding

All calculations were performed in BIOVIA's Discovery Studio Version 3.5. The crystal structure of S1R in complex with *N*-(1-benzylpiperidin-4-yl)-4-iodobenzamide (code 5HK2 in PDB protein data base) was retrieved from the PDB. Prior to docking, the protein structure was prepared using the prepare protein protocol. Docking was performed with the CDOCKER program using default parameters. Confirmation of S1R binding was performed by *in vitro* competitive displacement-binding assay using the known S1R binder [³H]-haloperidol (Ganapathy et al., 1999). The test was executed by Eurofin Central Laboratory Inc.

Image-Based Single Cell Analysis

MEFs were seeded on 1% gelatin-coated 96-well plate at a density of 5000 cells per well. Twenty-four hours post-plating cells were incubated with the tested compounds for 24 h. Several DMSO-treated cells (control) were included in each plate at different locations. The cells were then stained by addition of fluorogenic dyes for further incubation for 30 min at 37°C. Hoechst 33258 (#861405; Sigma-Aldrich) and JC-1 (#T4069; Sigma-Aldrich) were used at final concentration

of 2 μ g/ml; CellTrace CFSE (#C345545; Molecular Probes), and CellROX Deep Red (#C10422; Molecular Probes) at final concentration of 5 μ M. CellROX was used together with Hoechst and CFSE; JC1 was used together with Hoechst. Cells were washed with Hank's balanced salt solution (HBSS) used for images acquisition by IN Cell Analyzer 2000 (GE Healthcare, Pittsburgh, PA, United States). IN Cell Developer Toolbox 1.9.1 software (GE Healthcare, Pittsburgh, PA, United States) served for analysis. Analysis included cells segmentation using Hoechst and/or CFSE signals. For analysis of JC1 staining, integrated intensity of green and red emissions served for detection of damaged and intact mitochondria, respectively.

Cell Survival Assay

Cells were seeded on 96-well plate at a density of 5000 cells per well. Astrocytes were seeded following coating with 0.001% PDL. Twenty-four hours post-plating cells were incubated with the tested compounds for 24 h followed by staining with 0.1% crystal violet/4% formaldehyde/1% ethanol as described in Heiss et al. (2014).

Quantification of Gli1 mRNA

Total RNA was subjected to reverse transcription using qscript cDNA synthesis kit (#95047 Quanta Biosciences) and subjected to qPCR analysis using SYBR-Green (PerfeCTa[®] SYBR[®] Green FastMix[®], ROXTM; #95073; Quanta Biosciences) and the following oligonucleotide primers: Gli1 Fwd 5'-CCCATAGGGTCTCGGGTCTCAAAC-3' and Gli1 Rev 5'-GGA GGACCTGCGGCTGACTGTGTAA-3' for Gli1 mRNA amplification and Gapdh Fwd 5'-TGGCAAAGTGGAGATTGTT GCC-3' and Gapdh REV 5'-AAGATGGTGATGGGCTTCCCG-3' for Gapdh mRNA as an internal control. Equal amounts of RNA were used and reactions were carried out for 40 cycles in StepOne Real-time PCR apparatus (Applied Biosystems). Average relative quantity (RQ) was calculated by the $\Delta\Delta C_t$ method.

Luciferase Activity Assay

Sonic hedgehog-LIGHT2 cells were seeded at a density of 10,000 cells per well of a 96-well plate in growing medium. Twenty-four hours post-plating cells were incubated for 24 h with the tested compounds in low serum media (0.5%) without G418 and Zeocin. Following lysis, Firefly and Renilla luminescence was measured using the Dual Luciferase assay kit (Promega) and a Veritas microplate luminometer (Turner Biosystems).

Western Blot Analysis

10⁵ Astrocytes or 1.5 * 10⁵ MEFs were seeded per well of a six-well plate and cultured for 3 or 2 days, respectively. After one wash with PBS, 100 μ l of lysis buffer containing 1.6% SDS, 80 mM DTT, 8% glycerol, 64 mM Tris pH 6.8 were applied directly on the cell monolayer followed by extract collection. Forty microliters per lane of MEFs total cell extract, 10 μ l per lane of astrocytes total cell extract, or 30 μ g total protein per lane of

brain protein extract were separated by 15% SDS-PAGE followed by immunoblot analysis using antibodies specific for Sig1R (Santa Cruz #137075) and SDHB (Abcam #ab14714). The enhanced chemiluminescence signal was captured using a AI600 Imager (Amersham) and quantified by ImageQuant TL (GE Healthcare, Pittsburgh, PA, United States).

mtDNA Quantification

Total DNA was extracted using GenElute™ (#G1N350; Sigma-Aldrich) and used for real-time SYBR-Green-based PCR reactions (PerfeCTa® SYBR® Green FastMix®, ROX™; #95073; Quanta Biosciences) using 40 cycles in StepOne Real-time PCR apparatus (Applied Biosystems). The following oligonucleotide primers were used: 5'-ACCGCGTTCATACGATTAAC-3' and 5'-CCCAGTTTGGGTCTTAGCTG-3' (12SrRNAm FWD and 12SrRNAm REV, respectively, to amplify the gene encoding mitochondrial 12S rRNA); and 5'-CGCGGTTCTATT TTGTTGGT-3' and 5'-AGTCGGCATCGTTTATGGTC-3' (18SrRNAn FWD and 18SrRNAn REV, respectively, to amplify the nuclear gene encoding 18S rRNA). Average RQ of mtDNA per nucDNA values were calculated and normalized to the experimental control value.

TMRE Staining

MEFs were seeded at a density of 4×10^4 cells per well of a 24-well plate. Twenty-four hours post-plating the cells were incubated with the tested compounds for 6 h followed by staining with 200 nM tetra-methyl-rhodamine-ethyl esterperchlorate (TMRE) (Abcam) for 30 min at 37°C. Cells were removed by trypsinization, washed, and resuspended in PBS. $5-10 \times 10^3$ cells were analyzed by Stratadigm S1000EXi cell sorter and FlowJo software (FLOWJO, LLC, Ashland, OR, United States).

Oxygen Consumption

Oxygen consumption was measured in primary MEFs and astrocytes using a XF96 extracellular Flux Analyzer (Seahorse Bioscience, Billerica, MA, United States) as described (Invernizzi et al., 2012). Primary MEFs or astrocytes were seeded in a XF96-well cell culture microplate at a density of 5000 cells/well and incubated for 24 or 72 h, respectively, in 80 μ L of MEF medium or astrocytes medium (#1801; Sciencell Research Labs), at 37°C in 5% CO₂ atmosphere prior to analysis. The Mito Stress Test Kit (Agilent Technologies, Santa Clara, CA, United States) was used to measure oxygen consumption rate (OCR) as detailed in Raini et al. (2017). ATP-linked respiration and maximal capacity respiration were determined as recommended by the supplier. Oligomycin (Sigma, #O4876) was used at concentrations of 1 μ M for MEFs and 2 μ M for astrocytes; FCCP (#C2920, Sigma) at 1.5 μ M, antimycin A (#A8674, Sigma) at 0.5 μ M for MEFs and 1 μ M for astrocytes; and rotenone (#R8875, Sigma) at 0.5 μ M for MEFs and 1 μ M for astrocytes. MEFs data were normalized to mtDNA/nucDNA content. Astrocytes data were normalized to cell number, obtained by Crystal Violet staining (Heiss et al., 2014).

Statistics

For all comparisons, Student's *t*-test was performed using more than or equal to three independent biological repeats for each group (methodological selection of sample size was not applied).

RESULTS

Selection of Library and Screening of Compounds

A computational workflow for rational selection of an optimal screening library (Gilad et al., 2015) was applied to the analysis of nine commercially available libraries containing ~380,000 compounds. We ranked the libraries based on three criteria: (1) Absorption, Distribution, Metabolism, Excretion, and Toxicity (commonly abbreviated ADME/T) profiling. This pharmacokinetic profile is of paramount importance in determining the fate of a compound within the body and consequently its drug-like properties. As part of this profiling, we developed a new Quantitative Structure Activity Relationship (QSAR) model for the prediction of blood brain barrier permeability. Briefly, QSAR models are mathematical equations correlating activities with structure-based descriptors for a set of compounds; (2) internal diversity; and (3) similarity to the known active compound Guanabenz. We included the third criteria because Guanabenz was proposed to inhibit PPP1R15A, a stress-induced subunit of protein phosphatase 1 (PP1), responsible for eIF2 α dephosphorylation (Tsaytler et al., 2011). This information was relevant for us since a genetic knockout of PPP1R15A gene corrected the VWM phenotype of Eif2b5^{R132H/R132H} mice (unpublished data). Importantly, by using non-phosphorylatable eIF2 α (eIF2 α ^{S51A}) cells, a recent study challenged the fact that Guanabenz interferes with PPP1R15A-mediated eIF2 α -P dephosphorylation (Crespillo-Casado et al., 2017). However, Bergmann glia pathology and cerebellar myelin pathology improved with Guanabenz treatment in mice (Dooves et al., 2018).

All three criteria were combined into a single library score using a consensus approach while assigning equal weights to each. The rankings based on the individual criteria and the consensus rankings are presented in **Table 1**. These results indicate that the DIVERSet™-EXP library by Chembridge was the best screening library for the current project.

For screening, we took advantage of the differential cellular phenotypic characteristics of primary mouse embryonic fibroblasts (MEFs) isolated from Eif2b5^{R132H/R132H} mouse model (Geva et al., 2010) and based the assay on their abnormally high mitochondria content. This approach was chosen because our previous study have shown that increased mitochondrial biogenesis in eIF2B-mutant MEFs is a compensatory response to overcome compromised oxidative phosphorylation (Raini et al., 2017). We hypothesized that incubation of mutant cells with a compound leading to enhanced mitochondrial function will alleviate their need to increase mitochondria content. Since our cellular assay relies on small differences in mitochondrial function, it became apparent that medium throughput screening

TABLE 1 | Library ranking.

Library	Size	ADME/T ranking	Diversity ranking	Similarity ranking	Final rank
Elite Libraries	70,114	2	8	8	8
Platinum Collection	113,962	6	7	5	8
DIVERSet TM -CL	50,000	2	4	7	5
DIVERSet TM -EXP	50,000	1	5	1	1
Drug-Like Set	20,160	3	2	3	2
Pharmacological Diversity Set	10,240	3	6	6	6
Maybridge Screening Collection	54,318	4	3	2	3
Prestwic Chemical Library [®]	1,280	7	1	9	7
MSII Full Library	10,000	5	2	4	4

employing several repeats with several batches of cells is likely to give much better results than high-throughput screening. This required reducing the number of compounds tested at each cycle. We anticipated that experimental testing of a subset of compounds, which well represents the entire parent library (i.e., a representative subset), should provide a similar amount of information as would be provided by testing the entire library. This hypothesis stems from the similar property principle, which states that similar compounds have similar properties. We therefore clustered the DIVERSetTM-EXP library into 500 clusters and selected a single representative from each cluster, closest to the cluster center. Following biological testing, active hits easily traced back to their parent clusters. Testing additional members of “active clusters” provided valuable SAR information.

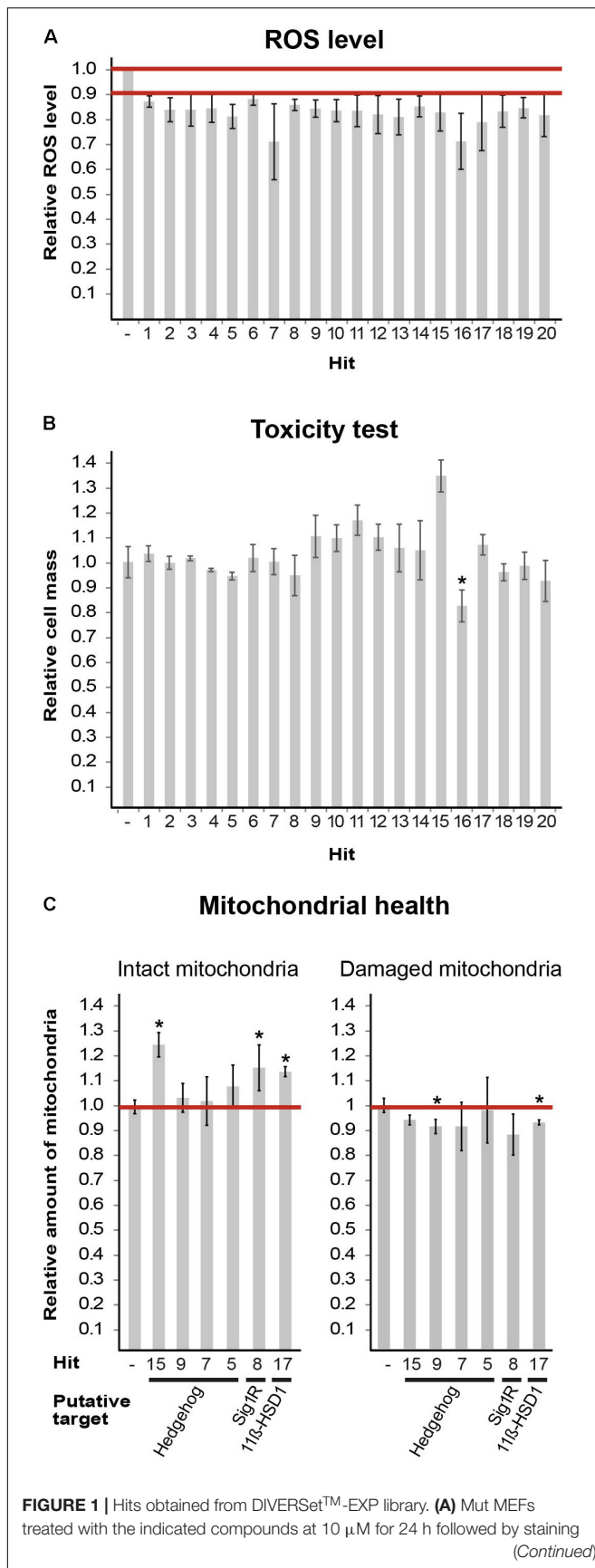
To assay the compounds, we used *cellROX*, a reactive oxygen species (ROS) fluorescent detector and a preferred *in situ* mitochondria content detector, for single cell-based imaging analysis as detailed previously (Raini et al., 2017). Briefly, the median *cellROX* integrated intensity of non-treated cells was set as a threshold to define the population above it, as “high-ROS cells.” This fraction, being 50% in non-treated cells, was set as 1. We expected it to be <1 if a compound acts via one of numerous possible mechanisms to decrease ROS levels. A compound was considered a “hit” if it was able to decrease the size of “high-ROS cells” population to 0.9 or below, in at least three independent experiments. The first screening round identified eight hits, each representing a different cluster. In the second round, we screened 437 compounds that were included in the eight relevant clusters and identified 20 hits, termed H1–H20 (Figure 1A; see chemical names in Table 2). We evaluated compound toxicity by testing cell survival following 24 h incubation with 10 μ M of each compound using crystal violet staining (Figure 1B). Only H16 has led to a significant decrease in cell viability and therefore not used for further analyses.

Next, we set to find putative targets of the identified hits by searching the Scifinder[®] database for structure similarities between the hits and other compounds with known targets/signaling pathways. Six hits were mapped to three putative targets/pathways: Shh, S1R, and 11 β -hydroxysteroid dehydrogenase type1 (11 β -HSD1). We further tested them for their ability to enhance mitochondrial health using JC-1 fluorescence staining. Based on membrane potential, JC-1 red and green emissions serve as proxy of intact and damaged

mitochondria, respectively. Treatments with hits H8 (putative target: S1R), H15 (putative target: Shh), and H17 (putative target: 11 β -HSD1) have led to increased level of intact mitochondria, while H9 and H17 treatment also decreased the level of damaged mitochondria (Figure 1C). To set the ground for further drug development we sought to confirm the predicted anomaly of Shh and S1R functions in eIF2B5-mutant primary MEFs.

Sonic Hedgehog (Shh) Pathway Regulation Is Impaired in Eif2b5^{R132H/R132H} Mutant Mice

Sonic hedgehog is an important morphogen for central nervous system patterning during development. Among its non-patterning functions is proliferation of oligodendrocytes precursors and their further differentiation (Fuccillo et al., 2006). While Shh activity increases during initial stages of brain development to induce oligodendrocyte proliferation and maturation, later on it decreases to allow complete differentiation and myelination (Bousslama-Oueghlani et al., 2012). Shh signaling is also involved in enhanced mitochondrial health (Wu et al., 2009; Malhotra et al., 2016). To assess the involvement of Shh pathway in VWM disease, we measured by RT-qPCR the mRNA level of *Gli1*, a Shh target gene. We used brain extracts of WT and Eif2b5^{R132H/R132H} mutant mice at postnatal ages of P18 and P21, the peak of oligodendrocyte differentiation and myelin formation in mice (Verity and Campagnoni, 1988). The normal expected decrease between P18 and P21 observed in WT was more prominent in mutants. Specifically, mutants showed significantly higher and lower levels at P18 and P21, respectively, compared to WT controls (Figure 2A). Our putative target identification analysis suggested Shh signaling pathway for four hits (H5, H7, H9, and H15). To test this prediction, we used Shh-lightII cells, which enable a read-out of Shh activation. These cells stably express *Renilla-Luciferase* for normalization purposes and an inducible *Firefly-Luciferase* reporter gene under the control of *Gli1* promoter (Taipale et al., 2000). We found that only H15 was able to activate Shh signaling pathway, as it led to increased *Firefly/Renilla luciferase* expression in a concentration-dependent manner (Figure 2B). Therefore, we concluded that H15 is a putative Shh agonist. To test if the rest of the compounds affect Shh pathway as antagonists, we tested their ability to inhibit the activity of a known potent *Smoothened*

**FIGURE 1 |** Continued

with fluorogenic dyes and image-based single-cell analysis. Shown is average effect on ROS level of 20 final hits (Table 2) from at least three-independent experiments \pm SEM. All values are statistically significant, $p < 0.02$. The extreme SEM points of all values are below the 90% cut-off; therefore, the actual average reduction is between 12 and 29%. (B) Mut MEFs were incubated or not for 24 h with 10 μ M of the indicated compound (Table 2) followed by crystal violet staining. Shown is average absorbance at OD = 570 nm as a proxy of cell mass, compared to cells in the absence of any compound, of three independent experiments \pm SEM, $*p = 0.0003$. (C) Mut MEFs were incubated or not for 24 h with 10 μ M of the indicated compound (Table 2) followed by JC1 and Hoechst staining. Image-based single-cell analysis using JC1 red and green emission employed to detect intact and damaged mitochondria, respectively. Values of untreated cells were set as 1. Shown are average values of at least three independent experiments for each parameter compared to its matching control \pm SEM. $*p < 0.05$. Putative targets are indicated.

agonist (SAG) (Chen et al., 2002). H5 and H7 inhibited the SAG-induced Shh activity in a concentration-dependent manner, confirming their involvement in this pathway as antagonists (Figure 2C). To confirm the ability of both Shh agonists and antagonists to improve mitochondrial health, we tested the effect of cyclopamine (a known Shh antagonist) and SAG (agonist) on JC-1 staining. Interestingly, both SAG and cyclopamine led to beneficial effects on mitochondrial health (Figure 2D).

Sigma-1-Receptor (S1R) Putative Target: Relevance and Efficacy Confirmation of H8 Binding to S1R

Sigma-1-Receptor is a transmembrane chaperone protein located at the ER-mitochondria interface, where it regulates their cross talk and function to promote cellular survival. Among many functions, it ensures Ca^{2+} signaling from the ER into the mitochondria by chaperoning IP3 receptor (Hayashi and Su, 2007). S1R role is important for multiple cellular scenarios including astrocytes activation and oligodendrocyte proliferation, differentiation, and myelin production (Demerens et al., 1999; Lisak et al., 2014; Zhang et al., 2015). As VWM disease is associated with mitochondria malfunction (Elroy-Stein, 2017; Raini et al., 2017) and since the hallmark of the pathology is related to impaired astrocytes activation, oligodendrocytes differentiation, and myelin formation (Schiffmann and Elroy-Stein, 2006; Dooves et al., 2016), we deduced that S1R might be involved in the disease. Moreover, given the similarity of H8 structure to a known S1R ligand (Lan et al., 2014), we reasoned that H8 may also be an S1R ligand. To test this possibility, we first computationally checked whether H8 is a potential binder of S1R by docking simulations using the CDOCKER program (Wu et al., 2003) as implemented in BIOVIA's Discovery Studio (2016). Initially, we tested whether CDOCKER can reliably reproduce the ligand-binding mode of a known binder, using the crystal structure of S1R in complex with *N*-(1-benzylpiperidin-4-yl)-4-iodobenzamide (code 5HK2 in the PDB protein data bank). Indeed, the lowest energy-binding mode obtained with CDOCKER had a root mean square value (RMSD) of 0.8 Å with respect to the crystal structure, suggesting that the program is appropriate for this study. Next, nine S1R binders with known

TABLE 2 | Hits and analogs.

ID	Chemical name
Hits	
H1	5-Benzyl-2-[(2-chlorophenyl)imino]-1,3-thiazolidin-4-one
H2	5-Butyl-3-[[2-(4-morpholinyl)ethyl]thio]-5H-[1,2,4]triazino[5,6-b]indole
H3	2-Phenyl- <i>N'</i> -[(5-[3-(trifluoromethyl)phenyl]-2-furyl)methylene]acetohydrazide
H4	1-{3-[(4-Chlorobenzyl)oxy]phenyl}ethanone
H5	1-Allyl-2-(3,4,5-trimethoxyphenyl)-1H-benzimidazole
H6	7-(Difluoromethyl)- <i>N</i> -[2-(4-morpholinyl)ethyl]-5-phenylpyrazolo[1,5- <i>a</i>]pyrimidine-3-carboxamide
H7	1-Phenyl-4-[4-(2-thienylcarbonyl)-1-piperazinyl]phthalazine
H8	4-[5-(3-Methylphenoxy)pentyl]morpholine
H9	1-(2-Fluorophenyl)-4-(phenylacetyl)piperazine
H10	2-[[2-Oxo-2-(1-piperidinyl)ethyl]thio]-4-phenyl-6-(trifluoromethyl)pyrimidine
H11	<i>N</i> -[2-(Phenylthio)cyclohexyl]benzenesulfonamide
H12	1-[[3-(Benzoyloxy)phenyl]carbonothioyl]-4-methylpiperazine
H13	5-Phenyl- <i>N</i> -(2-thienylmethyl)-7-(trifluoromethyl)pyrazolo[1,5- <i>a</i>]pyrimidine-2-carboxamide
H14	2-(2,3-Dihydro-9H-imidazo[1,2- <i>a</i>]benzimidazol-9-yl)-1-(4-hydroxyphenyl)ethanone hydrobromide
H15	1-Allyl-2-(2-phenylvinyl)-1H-benzimidazole
H16	2-[[2,5-Dimethoxyphenyl]diazenyl]-1-Methyl-1H-benzimidazole
H17	2-[[2,6-Dimethyl-1-piperidinyl]carbonyl]-7-methyl-5-phenylpyrazolo[1,5- <i>a</i>]pyrimidine
H18	2-(4-Morpholinylmethyl)-1-(1-naphthylmethyl)-1H-benzimidazole
H19	2-(Benzylthio)- <i>N</i> -cyclopentylbenzamide
H20	5-Isopropyl- <i>N</i> -methyl-3-phenylpyrazolo[1,5- <i>a</i>]pyrimidin-7-amine
Analog	
H8-1	4-[5-(3,5-Dimethylphenoxy)pentyl]morpholine
H8-2	4-[5-(3,4-Dimethylphenoxy)pentyl]morpholine
H8-3	4-[6-(3-Methylphenoxy)hexyl]morpholine
H8-4	4-[4-(3-Methylphenoxy)butyl]morpholine
H8-5	4-[4-(3,4-Dimethylphenoxy)butyl]morpholine
H8-6	4-[5-(3-Methoxyphenoxy)pentyl]morpholine
H8-7	4-[5-(3-Chlorophenoxy)pentyl]morpholine
H8-8	1-[5-(2-Fluorophenoxy)pentyl]-4-methylpiperazine

ligand–protein binding K_i values retrieved from PubChem¹ were docked into the S1R structure. The scores of the top ranked pose of each ligand correlated with the experimental K_i values and a significant correlation with $r^2 = 0.7$ was obtained (Figure 3). Next, hit H8 docked into this structure got a score of 49.38 kcal/mol, which falls within the range of scores for the known binders. To confirm the binding of hit H8 to S1R, we employed an *in vitro* competitive displacement-binding assay using the known S1R binder [³H]-haloperidol (Ganapathy et al., 1999). This test revealed that 10 μ M of H8 inhibited 92% of Haloperidol binding, confirming that H8 (see chemical name in Table 2) is a direct S1R binder.

Decreased S1R Expression in Eif2b5^{R132H/R132H} Mutant Mice

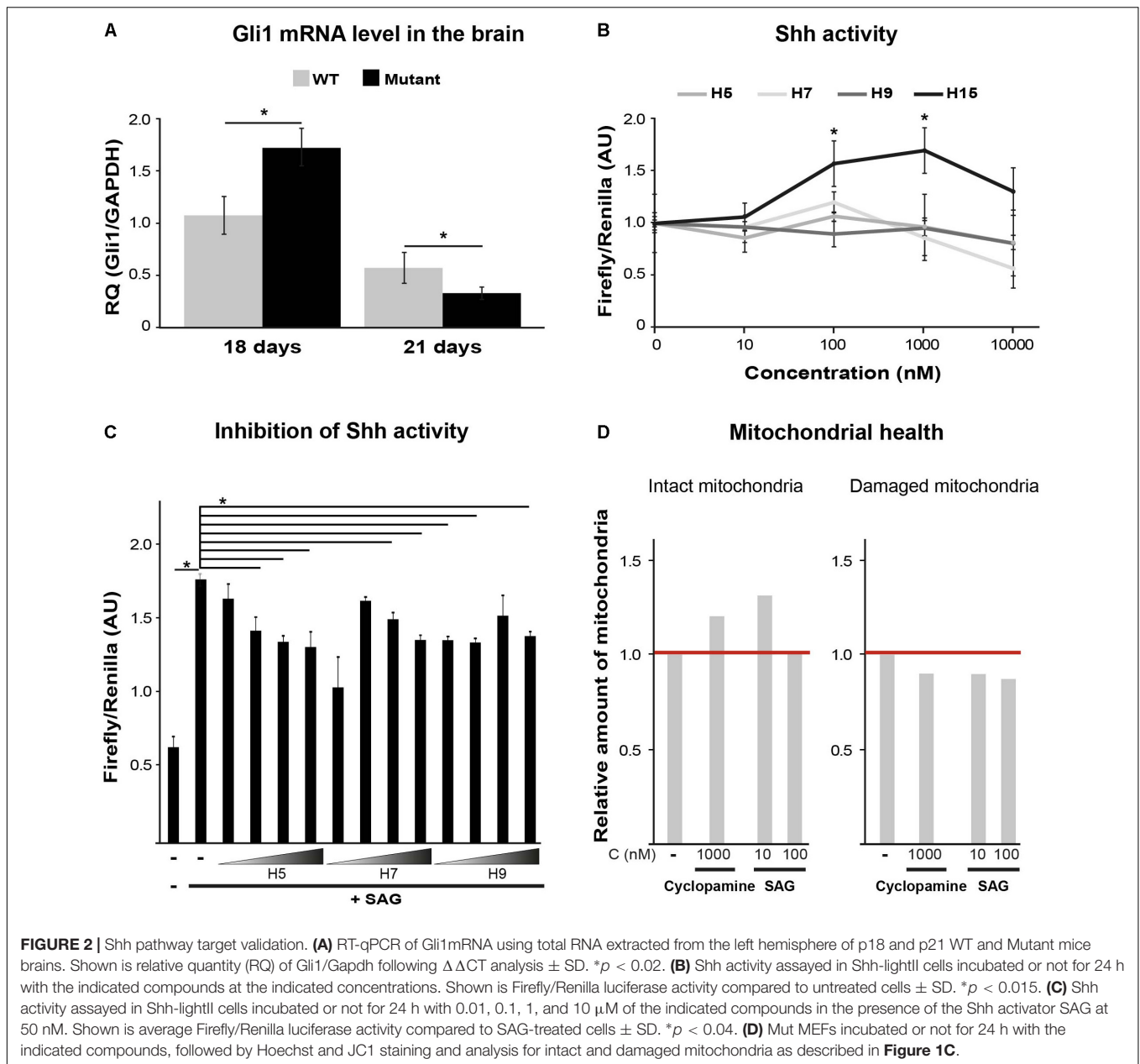
To set the ground for further drug development toward S1R as a relevant target we first tested if there is any VWM-related abnormality in S1R expression level. We recently discovered that primary MEFs and astrocytes isolated from Eif2b5^{R132H/R132H} mice suffer from oxidative respiration defects, leading to

increased mitochondrial biogenesis for compensation purposes to meet energetic needs (Raini et al., 2017). It was therefore important to test S1R protein level per mitochondria content. For this purpose, we tested the ratio between S1R protein level and the level of nuclear-encoded SDHB protein, a component of the mitochondrial electron transfer chain (ETC) complex. Western blot analysis revealed that primary MEFs and astrocytes isolated from mutant mice express 17 and 22% lower S1R/SDHB protein ratio compared to WT MEFs and astrocytes, respectively (Figures 4A,B). Brain extracts of mice at postnatal ages of P14–P18 showed S1R/SDHB levels lower by 34–35% compared to WT controls (Figure 4C).

Effect of S1R Binders on Abundance and Function of Mitochondria in Eif2b5^{R132H/R132H} MEFs and Astrocytes

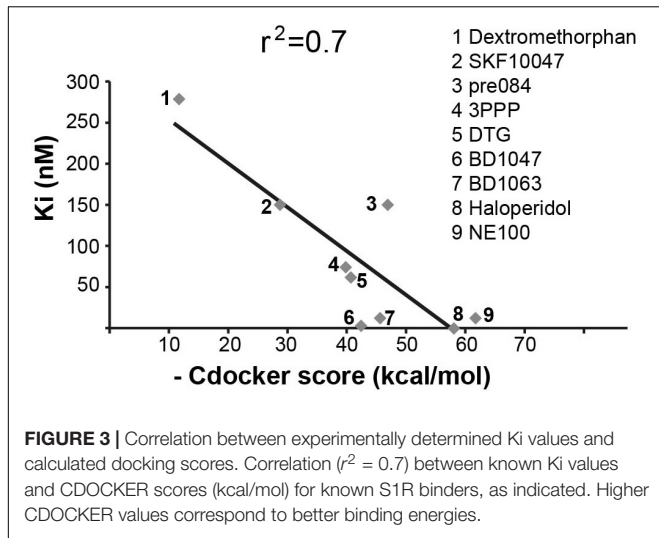
To further analyze the involvement of S1R in VWM disease, we tested the effect of Pre084 and NE-100, known S1R agonist and antagonist, respectively, on mitochondria content in primary MEFs isolated from Eif2b5^{R132H/R132H} mice. In addition to hit H8, the effect of pridopidine was also tested due to its high affinity to S1R (Sahlholm et al., 2015) and its beneficial effects on a

¹<http://pubchem.ncbi.nlm.nih.gov>



mouse model of Huntington disease, another neurodegenerative pathology (Ryskamp et al., 2017). Incubation for 6 h with 1 μ M of Pre084 corrected the abnormal high mitochondria content in mutant MEFs and brought it closer to WT level. A similar effect was observed for pridopidine and H8, suggesting that H8 functions as a S1R agonist (**Figure 5A**). In contrast to these results, NE-100 did not decrease the mitochondria content of mutant MEFs, i.e., did not correct their anomaly. The lack of any negative effect on survival of mutant MEFs upon incubation with as high as 30 μ M of Pre084, pridopidine, or H8 (**Table 3**), ruled out decreased mitochondria content due to a toxic effect. To verify that decreased mitochondria content is due to a repair effect, we stained the cells with TMRE, a positively charged

fluorescent dye specific for active mitochondria with membrane potential above a certain threshold (Crowley et al., 2016). While incubation of mutant MEFs for 6 h with 1 μ M of NE-100 dramatically decreased TMRE staining, similar concentration of Pre084, H8, and pridopidine did not lead to such a toxic outcome (**Figure 6**). Moreover, 1 μ M of H8 and 10 μ M of pridopidine increased TMRE staining and brought it to the level of untreated WT cells. The lower mitochondria content in S1R agonists-treated MEFs (**Figure 5A**) is consistent with the idea that S1R agonists positively affect membrane potential by elevating mitochondrial Ca^{2+} concentration, resulting in upregulation of the entire oxidative phosphorylation machinery for more efficient ETC activity and higher ATP synthesis (Brookes et al.,

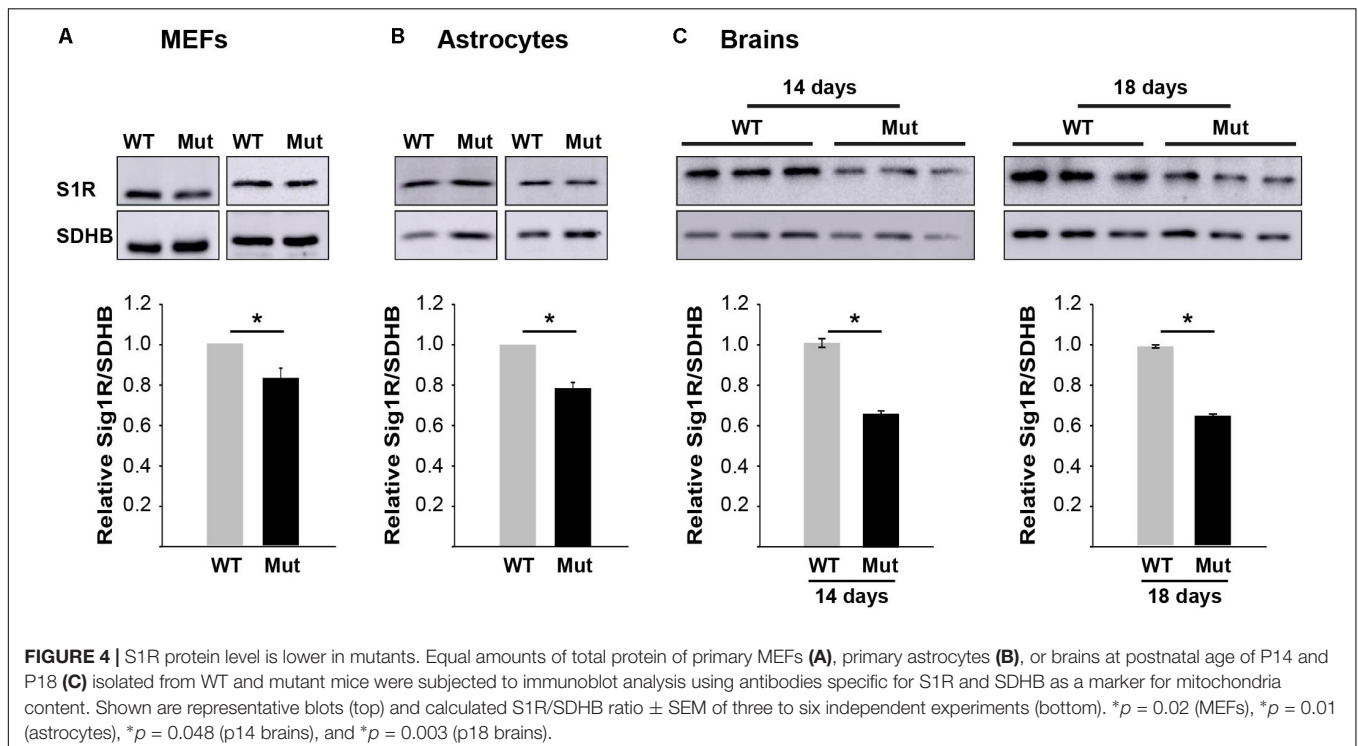


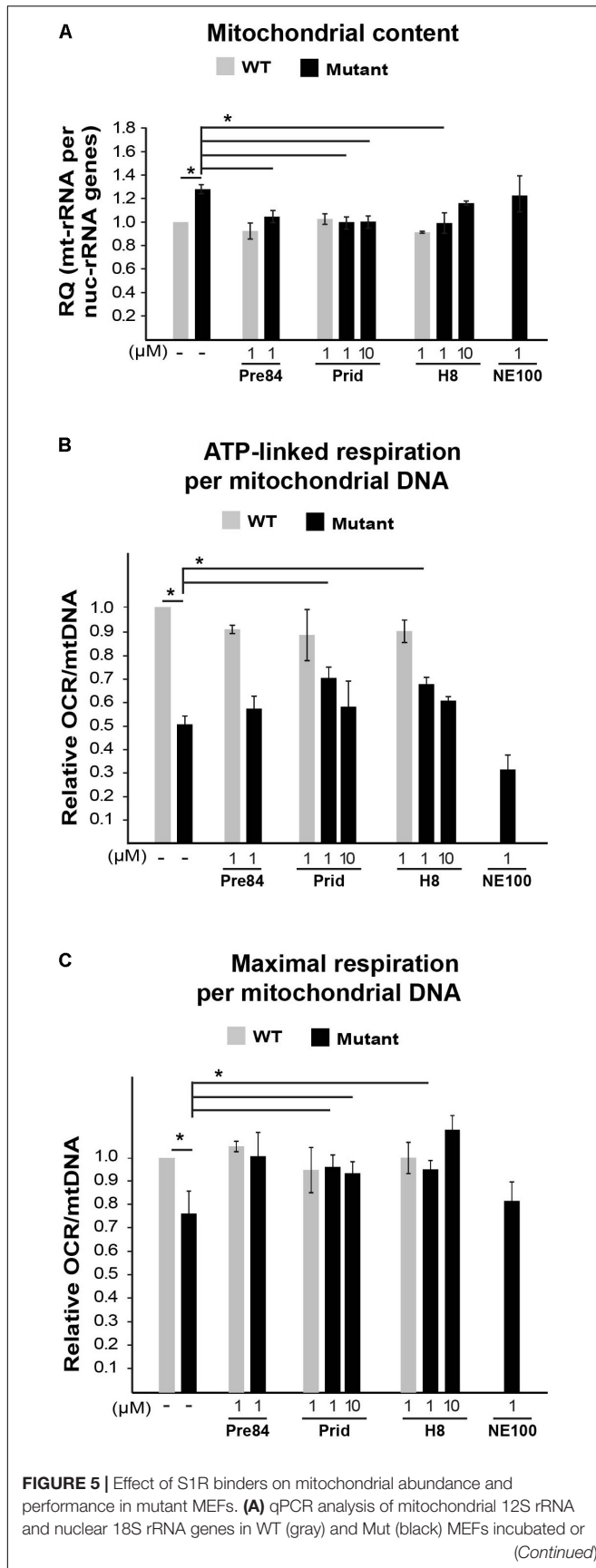
2004). To test if mitochondria content normalization is a result of enhanced oxidative respiration, we measured oxygen consumption rate (OCR). While NE-100 prompted a negative effect, S1R agonists did not elicit any effect on respiration per cell (not shown). However, given that H8 and pridopidine lead to decreased mitochondria content and increased mitochondrial membrane potential (Figures 5, 6), we normalized the OCR data to mitochondrial DNA content and revealed a statistically significant increase in ATP-linked and maximal respiration rates per mitochondria in mutant MEFs following incubation with 1 μ M H8 or pridopidine (Figures 5B,C).

Next, due to the specific involvement of astrocytes in VWM disease, it was important to test the effect of S1R agonists on primary astrocytes isolated from $Eif2b5^{R132H/R132H}$ mutant mice. Interestingly, while 1 or 10 μ M Pre-084, pridopidine, or H8 increased both ATP-linked and maximal respiration in mutant astrocytes (Figures 7B,C), no effect on mitochondria content per cell was observed (Figure 7A). This phenomenon is consistent with the beneficial outcome of S1R agonists, yet the partial correction of the anomaly in astrocytes is consistent with the high energetic requirements of these cells.

Effect of S1R Binders on Sensitivity of $Eif2b5^{R132H/R132H}$ MEFs and Astrocytes to ER Stress

Primary fibroblasts isolated from VWM patients are hypersensitive to pharmacologically induced ER stress (Kantor et al., 2005). The hypersensitivity of mutant MEFs isolated from $Eif2b5^{R132H/R132H}$ mice was confirmed by their lower survival rate compared to WT controls upon 22 h incubation with the ER stress agent Tunicamycin (Tun), as assayed by crystal violet staining (Figure 8A). Since S1R is involved in ER function, we sought to test whether hit H8 affects cell survival under ER stress conditions. Pre-treatment with 20 μ M H8 for 2 h followed by its presence throughout 22 h incubation with Tun increased the survival of mutant MEFs to the same rate of Tun-treated WT MEFs in the absence of H8, demonstrating its ability to rescue the ER hypersensitivity of mutants (Figure 8A). 30 μ M Pre084 was also able to rescue mutant MEFs from Tun-induced ER stress-mediated cell death (Figure 8B). Importantly, primary astrocytes isolated from $Eif2b5^{R132H/R132H}$ mice exhibited



**FIGURE 5 |** Continued

not with the indicated compounds for 6 h. Shown is average RQ of mtDNA per nucDNA values of two to seven independent experiments normalized to untreated WT ± SEM. **p* < 0.03. **(B,C)** Oxygen consumption rate (OCR) in WT and Mut MEFs incubated or not with the indicated compounds for 6 h. Values of ATP-linked respiration **(B)** and maximal respiration **(C)** analyzed and normalized to mtDNA per nucDNA values obtained in **(A)**. Shown are average values normalized to untreated WT MEFs ± SEM of six replicates in a representative experiment of three independent experiments. **p* < 0.05.

hypersensitivity to ER stress compared to astrocytes isolated from WT control mice. While S1R agonists did not rescue WT astrocytes, 30 μM pridopidine and 20–50 μM H8 increased the survival rate of mutant astrocytes under induced ER stress conditions (Figure 8C).

H8 Analogs

Taken together, the data indicate that treatment of mutant cells with S1R agonists (i.e., Pre084, pridopidine, and H8) leads to increased mitochondrial membrane potential, enhanced oxidative respiration, and increased ability of eIF2B5-mutant MEFs and astrocytes to cope with chronic ER stress. The finding that S1R expression level is low in primary MEFs, astrocytes, and brains isolated from *Eif2b5*^{R132H/R132H} mice suggests that S1R is a favorable potential target for the treatment of VWM disease and that compounds acting as S1R agonists such as Pre084, pridopidine, and hit H8 are plausible starting points for the development of relevant therapeutic strategy. To find a more potent starting point for drug development based on the current study, we set to identify structural analogs of H8. For this purpose, we scanned other EnamineStore and Chembridge libraries for compounds with structure similarity to that of H8. Eight similar analogs (listed in Table 2) were tested for their effect on mitochondrial health and cell survival following Tun-induced cell death. Five analogs elicited beneficial effect on mitochondrial health, as they increased the level of intact mitochondria while four of them also decreased the level of damaged mitochondria (Figure 9A). All the analogs exhibited a similar or better effect compared to H8 in the ER stress-induced cell death assay, as all increased cell survival. Analogs H8-2, H8-5, H8-6, and H8-7 displayed the most potent effect at 30 μM concentration (Figure 9B).

DISCUSSION

In the current study, we took advantage of the abnormal increased mitochondria content in *Eif2b5*^{R132H/R132H} primary MEFs (Raini et al., 2017), for screening of the DIVERSetTM-EXP library that contains 50,000 drug-like small molecules. The increased mitochondrial biogenesis, a compensatory response of mutant cells to their decreased oxidative phosphorylation, has set the rationale for our approach to assay mitochondria content by single cell-based imaging analysis. We reasoned that the decrease in mitochondria content in mutants could be the outcome of either toxic or healing scenario initiated by the tested compound. While the assay is simple,

TABLE 3 | Effect of compounds on cell survival.

			Survival (%) ± SEM		
		μM	Mut MEFs	WT astrocytes	Mut astrocytes
Sig1R binders	pre084	0.1	100 ± 2.1		
		1	101 ± 3.5	114 ± 7.9	97 ± 0.5
		10	99 ± 1.5	95 ± 2.3	93 ± 5.1
		20	97 ± 2.1		
		30	105 ± 1.9	82 ± 1.9 (<i>p</i> = 8.3E−04)	76 ± 4.9 (<i>p</i> = 0.03)
		50	80 ± 2.8 (<i>p</i> = 0.01)		
	Pridopidine	100	57 ± 2.2 (<i>p</i> = 1.5E−05)		
		0.1	102 ± 1.7		
		1	103 ± 1.3	103 ± 3.5	97 ± 2.7
		10	98 ± 1.6	101 ± 2.2	92 ± 2.8
		20	99 ± 0.64		
		30	99 ± 3.1	85 ± 4.3 (<i>p</i> = 0.02)	97 ± 5.0
	*H8	50	97 ± 1.2		
		100	91 ± 2.4 (<i>p</i> = 0.03)		
		0.1	104 ± 4.6		
1		102 ± 3.3	132 ± 10.7	108 ± 0.6	
10		99 ± 2.6	102 ± 3.8	93 ± 2.1	
20					
NE100	30	105 ± 13	99 ± 3.2	92 ± 1.6 (<i>p</i> = 0.14)	
	50				
	100				
	0.1	99 ± 2.1	98 ± 1.8		
H8 analogs	H8-1	1	98 ± 2.2	86 ± 1.1 (<i>p</i> = 1.5E−5)	94 ± 4.7
		10	88 ± 3.5 (<i>p</i> = 0.017)	79 ± 2.2 (<i>p</i> = 1.6E−4)	82 ± 4.3 (<i>p</i> = 0.01)
		30			65 ± 2.2 (<i>p</i> = 6.0E−06)
H8 analogs	H8-1	10	104 ± 2.7		
		20	103 ± 4.7		
		30	97 ± 3.9		
	H8-2	10	92 ± 4.2		
		20	94 ± 8.8		
		30	95 ± 13.1		
	H8-3	10	100 ± 7.2		
		20	96 ± 4.1		
		30	88 ± 4.5 (<i>p</i> = 0.09)		
	H8-4	10	92 ± 8.5		
		20	95 ± 4.2		
		30	98 ± 5.4		
	H8-5	10	92 ± 1.7		
		20	100 ± 4.4		
		30	98 ± 13.8		
	H8-6	10	97 ± 5.1		
		20	92 ± 1.1		
		30	93 ± 5.2		
	H8-7	10	98 ± 5.1		
		20	91 ± 4.7		
		30	88 ± 9.7 (<i>p</i> = 0.44)		
	H8-8	10	101 ± 5.6		
		20	99 ± 11		
		30	90 ± 3.5		

(Continued)

TABLE 3 | Continued

		Survival (%) ± SEM			
		μM	Mut MEFs	WT astrocytes	Mut astrocytes
Hedgehog modulators	SAG	0.01	98 ± 2.1		
		0.05	92 ± 3.2		
		0.1	95 ± 2.1		
	Cyclopamine	1	68 ± 2.7 (p = 1.9E-05)		
		0.1	92 ± 2.5		
		10	79 ± 1.4 (p = 0.02)		

Primary MEFs and astrocytes isolated from *Eif2b^{R132H/R132H}* (Mut) or WT mice were incubated for 24 h with the indicated compounds/concentrations followed by Crystal Violet staining. Cell survival of untreated cells was set to 100%. Shown is % cell survival ± SEM of at least three repeats. Toxicity refers to survival rate below 90% (marked gray, p-values indicated).

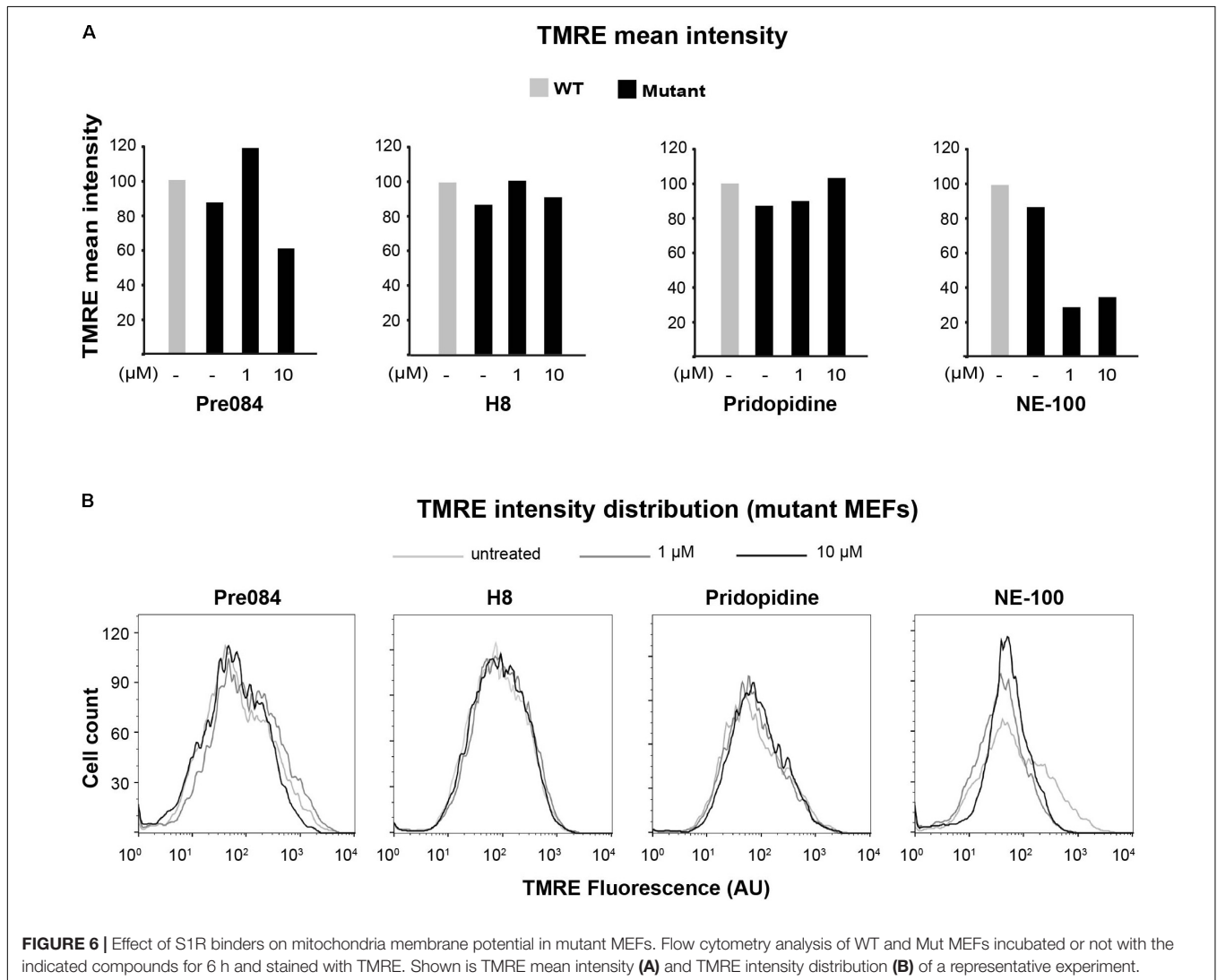
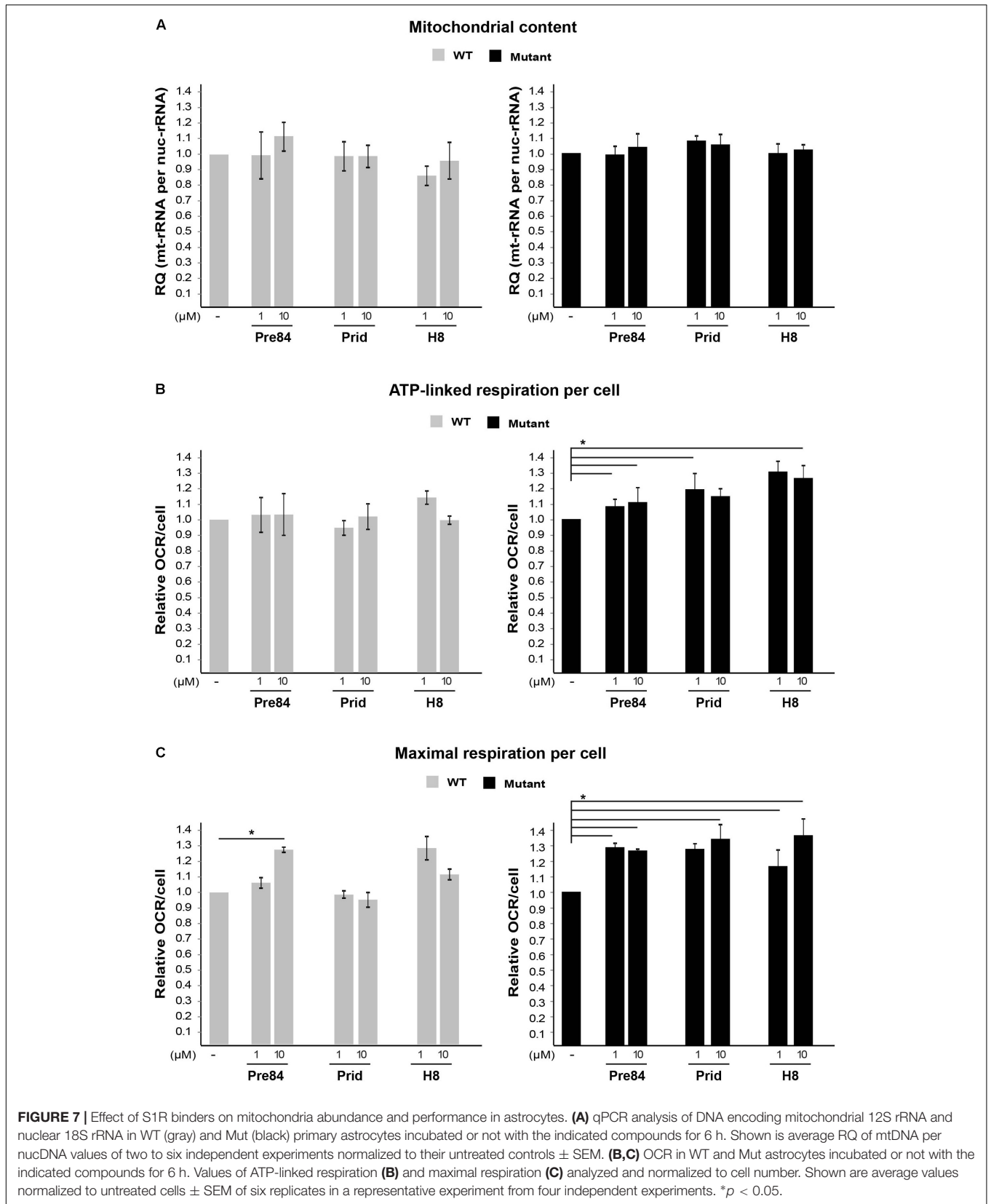


FIGURE 6 | Effect of S1R binders on mitochondria membrane potential in mutant MEFs. Flow cytometry analysis of WT and Mut MEFs incubated or not with the indicated compounds for 6 h and stained with TMRE. Shown is TMRE mean intensity (A) and TMRE intensity distribution (B) of a representative experiment.

it was associated with a major challenge. First, there is only 20–50% increase in mitochondria content in mutant compared to WT MEFs. Second, cellular metabolism and mitochondrial biogenesis are extremely sensitive to multiple

variables related to experimental conditions, some of which are beyond tight control. These limitations enforced us to avoid expensive high-throughput screening. Instead, we used rational computational approaches; first for the selection



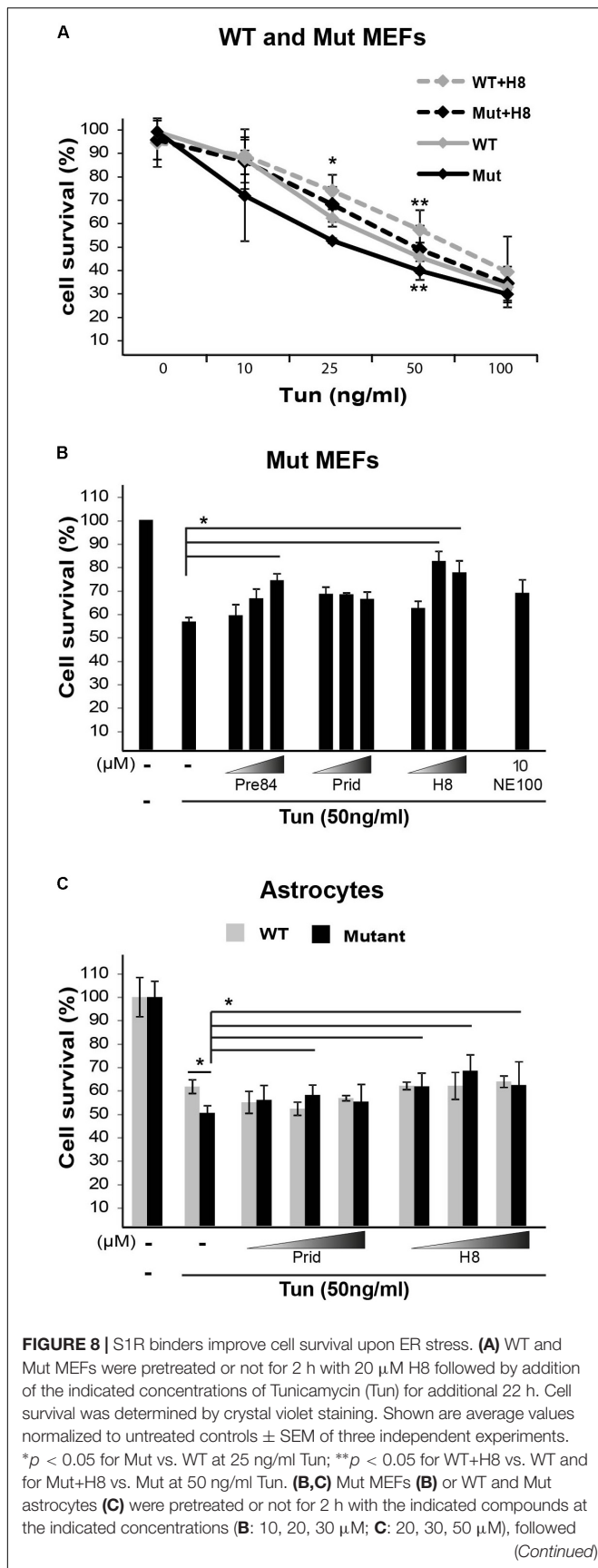
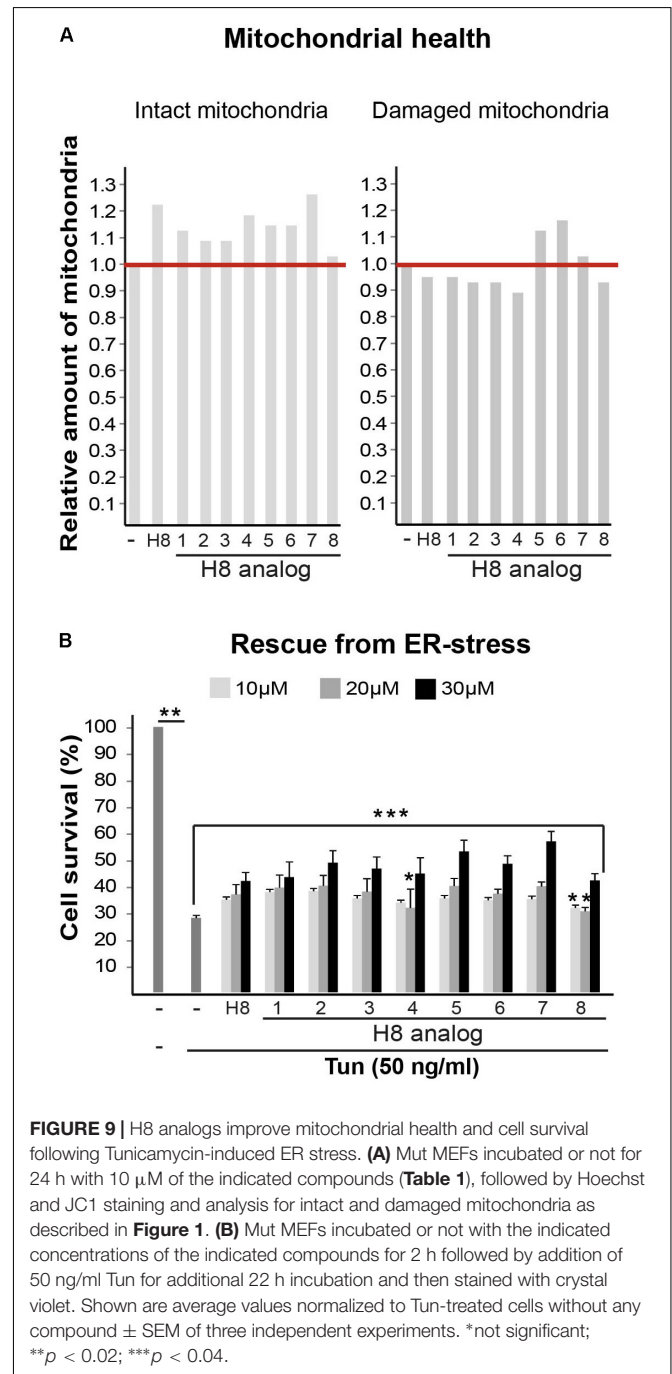


FIGURE 8 | Continued
by addition of 50 ng/ml Tun for additional 22 h and then stained with crystal violet. Shown are average values normalized to Tun-treated cells without any compound \pm SEM of three independent experiments, * $p < 0.05$.



of the optimal screening library, followed by its clustering based on structure similarities within its compounds. This strategy enabled us to minimize the number of compounds tested, thereby allowing for multiple repetitions of biological testing. Thus, we tested only 500 representative compounds in the

first round and ~500 most relevant compounds (consisting the members of the relevant positive clusters) in the second round, instead of the entire 50,000 compounds library. Surprisingly, only one hit (H16) decreased mitochondria content in mutant MEFs due to a toxic effect, while all other hit compounds reduced the need for mitochondrial biogenesis due to beneficial effects on mitochondrial health (**Figure 1**). Subsequent analysis of structural similarities between our primary hits and other compounds with known targets afforded the identification of three putative cellular pathways/targets: 11 β -HSD1, Shh, and S1R. This finding is significant by itself, as it is the first time these cellular components are mentioned in the context of VWM disease.

11 β -Hydroxysteroid dehydrogenase type 1 enzyme is widely expressed throughout the central nervous system. It regenerates active glucocorticoids from their inactive 11-keto derivatives and possesses 7 β -hydroxycholesterol dehydrogenases activity involved in oxysterol metabolism (Wyrwoll et al., 2011). The involvement of this enzyme in VWM disease is proposed since 7-ketocholesterol and 7 β -hydroxycholesterol cause phenotypic characteristics associated with the disease. These include ER stress, impaired mitochondrial function and increased ROS production which lead to apoptosis and autophagy in murine oligodendrocytes (Nury et al., 2015). The actual implication of 11 β -HSD1 in VWM pathology is yet to be determined.

Shh signaling pathway is involved in many cellular contexts and molecular mechanisms. The canonical scenario involves cell-surface binding of a ligand, leading to the formation of repressor or activator forms of the GLI/CI family members of zinc-finger transcription factors (Fuccillo et al., 2006). Shh activity is required for oligodendrocytes generation, maturation, and myelin formation during early brain development. The abnormal high and low Gli1 mRNA level at P18 and P21, respectively, in the brains of mutant mice, indicate abnormal Shh signaling due to the mutation in eIF2B during the peak of myelin formation (**Figure 2A**). This important observation, pointing at impaired programming of Shh pathway in mutants, is consistent with our previous finding related to delayed waves of gene expression during early brain development in Eif2b5^{R132H/R132H} mouse model (Marom et al., 2011). The impact of Shh signaling modulation on mitochondrial health in mutant MEFs (**Figure 2D**) further supports the relevance of Shh pathway to VWM pathology. Moreover, Shh signaling is required for the maintenance of endogenous adult neural stem cells (NSCs) which serve as a source for remyelination in the adult brain (Fuccillo et al., 2006). Interestingly, Samanta et al. (2015) reported that Gli1 inhibition enhances NSCs recruitment to demyelinated lesions and increases their differentiation into oligodendrocytes. Remarkably, the small molecule GANT61 successfully inhibits Gli1 and improves remyelination in an experimental animal model for multiple sclerosis (Samanta et al., 2015). Taken together, pharmacological targeting of the Shh signaling pathway may serve as a new therapeutic opportunity for the treatment of VWM disease. Demyelination is a hallmark of VWM pathology, thus additional work is required for characterization of Shh signaling pathway role in the etiology of the disease. Further effort will be necessary for elucidating the specific binding targets of

Shh-related compounds identified in this study (**Figure 2**). Once elucidated, compounds H5, H7, H9, and H15 may be attractive candidates for further drug development, for the treatment of VWM and additional demyelinating disorders.

Sigma-1-Receptor plays important roles in many physiological functions and known as a pluripotent modulator in living systems. While it resides in the mitochondria-associated ER membrane (MAM), it can also translocate to the plasma membrane to interact with ion channels and other receptors to affect their function, and interact with cytoplasmic soluble proteins. Furthermore, S1R can translocate to the nuclear envelope to recruit chromatin-remodeling factors and thereby affect the transcription of genes. S1R promotes cell survival under physiological stress conditions by regulating ER-mitochondria Ca²⁺ flux, signaling for antioxidants expression and attenuating free radicals damage (Su et al., 2016). The increase in ATP-linked and maximal respiration rates by S1R agonists treatment of mutant cells (**Figures 5, 7**) clearly indicates the beneficial effect of S1R activation in the context of VWM pathology. Not only that it enhances mitochondrial function most probably by modulating Ca²⁺ signaling, it also enhances the ability of mutant cells to cope with chronic ER stress (**Figure 8**), supposedly by activating the mitochondrion-ER-nucleus signaling axis, as previously reported, to counteract ER stress (Mori et al., 2013).

Due to the wide range of S1R effects on cellular physiology, it is not surprising that highly sensitive brain cells are profoundly dependent on its function. This includes astrocytes activation (Zhang et al., 2015), axon outgrowth (Li et al., 2017), oligodendrocyte proliferation, differentiation, and myelin production (Demerens et al., 1999; Lisak et al., 2014). Interestingly, S1R knockout mice display locomotor deficits associated with muscle weakness, axonal degeneration, and motor neuron loss because of affected intracellular calcium signaling, ER stress, and defects in mitochondrial dynamics due to dysfunctional ER-mitochondria crosstalk (Bernard-Marissal et al., 2015). The intense impact of S1R function on the central nervous system explains its involvement in multiple neurological disorders including Alzheimer's disease, major depressive disorders, and schizophrenia (Nguyen et al., 2017). Therefore, S1R activation is highlighted as neuroprotective and neurorestorative for various disorders (Ruscher and Wieloch, 2015; Li et al., 2017). The current work demonstrates for the first time the beneficial effect of S1R agonists on eIF2B-mutant cells. Together with the low S1R expression in mutants compared to controls (**Figure 4**), this study marks S1R as a strong therapeutic target for the development of a treatment for VWM disease. The cellular effect of several known S1R agonist molecules was already partially evaluated and classified (Maurice and Su, 2009). In the current study, we identified an additional S1R agonist, i.e., 4-[5-(3-methylphenoxy)pentyl]morpholine, and assayed eight analogs of this compound (**Figure 9** and **Table 2**) for their effect on mitochondrial function. These compounds serve as promising drug-like candidates for the development of a treatment for VWM disease as well as for other relevant central nervous system pathologies.

AUTHOR CONTRIBUTIONS

AA designed and performed experiments, interpreted data, organized and created figures, and helped with manuscript preparation. RS-E contributed to image-based screening and analyses. MH performed and interpreted astrocytes experiments, contributed to figures preparation, and manuscript editing. YG performed rational computational approaches. HS designed and guided computational approaches, critically discussed the data, and contributed to manuscript preparation. OE-S initiated, designed, and conducted the project, critically discussed the data, and wrote the manuscript.

REFERENCES

- Bernard-Marissal, N., Medard, J. J., Azzedine, H., and Chrast, R. (2015). Dysfunction in endoplasmic reticulum-mitochondria crosstalk underlies SIGMAR1 loss of function mediated motor neuron degeneration. *Brain* 138(Pt 4), 875–890. doi: 10.1093/brain/awv008
- BIOVIA Discovery Studio (2016). *Discovery Studio Modeling Environment Release 2017*. San Diego, CA: BIOVIA Discovery Studio.
- Bousslama-Oueghlani, L., Wehrle, R., Doulazmi, M., Chen, X. R., Jaudon, F., Lemaigre-Dubreuil, Y., et al. (2012). Purkinje cell maturation participates in the control of oligodendrocyte differentiation: role of sonic hedgehog and vitronectin. *PLoS One* 7:e49015. doi: 10.1371/journal.pone.0049015
- Brookes, P. S., Yoon, Y., Robotham, J. L., Anders, M. W., and Sheu, S. S. (2004). Calcium, ATP, and ROS: a mitochondrial love-hate triangle. *Am. J. Physiol. Cell Physiol.* 287, C817–C833. doi: 10.1152/ajpcell.00139.2004
- Cabilly, Y., Barbi, M., Geva, M., Marom, L., Chetrit, D., Ehrlich, M., et al. (2012). Poor cerebral inflammatory response in eIF2B knock-in mice: implications for the aetiology of vanishing white matter disease. *PLoS One* 7:e46715. doi: 10.1371/journal.pone.0046715
- Chen, J. K., Taipale, J., Young, K. E., Maiti, T., and Beachy, P. A. (2002). Small molecule modulation of Smoothed activity. *Proc. Natl. Acad. Sci. U.S.A.* 99, 14071–14076. doi: 10.1073/pnas.182542899
- Crespillo-Casado, A., Chambers, J. E., Fischer, P. M., Marciniak, S. J., and Ron, D. (2017). PPP1R15A-mediated dephosphorylation of eIF2 α is unaffected by Sephin1 or Guanabenz. *Elife* 6:e26109. doi: 10.7554/eLife.26109
- Crowley, L. C., Christensen, M. E., and Waterhouse, N. J. (2016). Measuring mitochondrial transmembrane potential by TMRE staining. *Cold Spring Harb Protoc.* 2016.pdb.prot087361. doi: 10.1101/pdb.prot087361
- Demerens, C., Stankoff, B., Zalc, B., and Lubetzki, C. (1999). Eliprodil stimulates CNS myelination: new prospects for multiple sclerosis? *Neurology* 52, 346–350.
- Dooves, S., Bugiani, M., Postma, N. L., Polder, E., Land, N., Horan, S. T., et al. (2016). Astrocytes are central in the pathomechanisms of vanishing white matter. *J. Clin. Invest.* 126, 1512–1524. doi: 10.1172/JCI83908
- Dooves, S., Bugiani, M., Wisse, L. E., Abbink, T. E. M., van der Knaap, M. S., and Heine, V. M. (2018). Bergmann glia translocation: a new disease marker for vanishing white matter identifies therapeutic effects of Guanabenz treatment. *Neuropathol. Appl. Neurobiol.* 44, 391–403. doi: 10.1111/nan.12411
- Elroy-Stein, O. (2017). Mitochondrial malfunction in vanishing white matter disease: a disease of the cytosolic translation machinery. *Neural Regen. Res.* 12, 1610–1612. doi: 10.4103/1673-5374.217329
- Elroy-Stein, O., and Schiffmann, R. (2015). “Vanishing white matter disease,” in *Rosenberg’s Molecular and Genetic Basis of Neurological and Psychiatric Disease*, eds R. N. Rosenberg and J. M. Pascual (London: Elsevier Inc.), 1015–1030. doi: 10.1016/B978-0-12-410529-4.00086-3
- Fogli, A., and Boesflug-Tanguy, O. (2006). The large spectrum of eIF2B-related diseases. *Biochem. Soc. Trans.* 34(Pt 1), 22–29. doi: 10.1042/BST0340022
- Fuccillo, M., Joyner, A. L., and Fishell, G. (2006). Morphogen to mitogen: the multiple roles of hedgehog signalling in vertebrate neural development. *Nat. Rev. Neurosci.* 7, 772–783. doi: 10.1038/nrn1990
- Ganapathy, M. E., Prasad, P. D., Huang, W., Seth, P., Leibach, F. H., and Ganapathy, V. (1999). Molecular and ligand-binding characterization of the

FUNDING

This work was funded by the ELA Foundation (grant ELA2012-013C2).

ACKNOWLEDGMENTS

We thank Miguel Weil and Leo Solmesky for the use of IN Cell Analyzer 2000 (GE Healthcare, Pittsburgh, PA, United States) and James Salzer for the kind gift of Shh-light2 cells.

- sigma-receptor in the Jurkat human T lymphocyte cell line. *J. Pharmacol. Exp. Ther.* 289, 251–260.
- Gat-Viks, I., Geiger, T., Barbi, M., Raini, G., and Elroy-Stein, O. (2015). Proteomics-level analysis of myelin formation and regeneration in a mouse model for Vanishing White Matter disease. *J. Neurochem.* 134, 513–526. doi: 10.1111/jnc.13142
- Geva, M., Cabilly, Y., Assaf, Y., Mindroul, N., Marom, L., Raini, G., et al. (2010). A mouse model for eukaryotic translation initiation factor 2B-leucodystrophy reveals abnormal development of brain white matter. *Brain* 133(Pt 8), 2448–2461. doi: 10.1093/brain/awq180
- Gilad, Y., Nadassy, K., and Senderowitz, H. (2015). A reliable computational workflow for the selection of optimal screening libraries. *J. Cheminform* 7:61. doi: 10.1186/s13321-015-0108-0
- Hayashi, T., and Su, T. P. (2007). Sigma-1 receptor chaperones at the ER-mitochondrion interface regulate Ca(2+) signaling and cell survival. *Cell* 131, 596–610. doi: 10.1016/j.cell.2007.08.036
- Heiss, E. H., Kramer, M. P., Atanasov, A. G., Beres, H., Schachner, D., and Dirsch, V. M. (2014). Glycolytic switch in response to betulinic acid in non-cancer cells. *PLoS One* 9:e115683. doi: 10.1371/journal.pone.0115683
- Invernizzi, F., D’Amato, I., Jensen, P. B., Ravaglia, S., Zeviani, M., and Tiranti, V. (2012). Microscale oxygraphy reveals OXPHOS impairment in MRC mutant cells. *Mitochondrion* 12, 328–335. doi: 10.1016/j.mito.2012.01.001
- Kantor, L., Harding, H. P., Ron, D., Schiffmann, R., Kaneski, C. R., Kimball, S. R., et al. (2005). Heightened stress response in primary fibroblasts expressing mutant eIF2B genes from CACH/VWM leukodystrophy patients. *Hum. Genet.* 118, 99–106. doi: 10.1007/s00439-005-0024-x
- Kashiwagi, K., Takahashi, M., Nishimoto, M., Hiyama, T. B., Higo, T., Umehara, T., et al. (2016). Crystal structure of eukaryotic translation initiation factor 2B. *Nature* 531, 122–125. doi: 10.1038/nature16991
- Lan, Y., Chen, Y., Xu, X., Qiu, Y., Liu, S., Liu, X., et al. (2014). Synthesis and biological evaluation of a novel sigma-1 receptor antagonist based on 3,4-dihydro-2(1H)-quinolinone scaffold as a potential analgesic. *Eur. J. Med. Chem.* 79, 216–230. doi: 10.1016/j.ejmech.2014.04.019
- Leegwater, P. A., Vermeulen, G., Konst, A. A., Naidu, S., Mulders, J., Visser, A., et al. (2001). Subunits of the translation initiation factor eIF2B are mutant in leukoencephalopathy with vanishing white matter. *Nat. Genet.* 29, 383–388. doi: 10.1038/ng764
- Li, D., Zhang, S. Z., Yao, Y. H., Xiang, Y., Ma, X. Y., Wei, X. L., et al. (2017). Sigma-1 receptor agonist increases axon outgrowth of hippocampal neurons via voltage-gated calcium ions channels. *CNS Neurosci. Ther.* 23, 930–939. doi: 10.1111/cns.12768
- Lisak, R. P., Nedelkoska, L., and Benjamins, J. A. (2014). Effects of dextromethorphan on glial cell function: proliferation, maturation, and protection from cytotoxic molecules. *Glia* 62, 751–762. doi: 10.1002/glia.22639
- Malhotra, A., Dey, A., Prasad, N., and Kenney, A. M. (2016). Sonic hedgehog signaling drives mitochondrial fragmentation by suppressing mitofusins in cerebellar granule neuron precursors and medulloblastoma. *Mol. Cancer Res.* 14, 114–124. doi: 10.1158/1541-7786.MCR-15-0278
- Marom, L., Ulitsky, I., Cabilly, Y., Shamir, R., and Elroy-Stein, O. (2011). A point mutation in translation initiation factor eIF2B leads to function- and time-specific changes in brain gene expression. *PLoS One* 6:e26992. doi: 10.1371/journal.pone.0026992

- Maurice, T., and Su, T. P. (2009). The pharmacology of sigma-1 receptors. *Pharmacol. Ther.* 124, 195–206. doi: 10.1016/j.pharmthera.2009.07.001
- Mori, T., Hayashi, T., Hayashi, E., and Su, T. P. (2013). Sigma-1 receptor chaperone at the ER-mitochondrion interface mediates the mitochondrion-ER-nucleus signaling for cellular survival. *PLoS One* 8:e76941. doi: 10.1371/journal.pone.0076941
- Motlekar, N., de Almeida, R. A., Pavitt, G. D., Diamond, S. L., and Napper, A. D. (2009). Discovery of chemical modulators of a conserved translational control pathway by parallel screening in yeast. *Assay Drug Dev. Technol.* 7, 479–494. doi: 10.1089/adt.2009.0198
- Nguyen, L., Lucke-Wold, B. P., Mookerjee, S., Kaushal, N., and Matsumoto, R. R. (2017). Sigma-1 receptors and neurodegenerative diseases: towards a hypothesis of sigma-1 receptors as amplifiers of neurodegeneration and neuroprotection. *Adv. Exp. Med. Biol.* 964, 133–152. doi: 10.1007/978-3-319-50174-1_10
- Nury, T., Zarrouk, A., Mackrill, J. J., Samadi, M., Durand, P., Riedinger, J. M., et al. (2015). Induction of oxiaoptophagy on 158N murine oligodendrocytes treated by 7-ketocholesterol-, 7beta-hydroxycholesterol-, or 24(S)-hydroxycholesterol: protective effects of alpha-tocopherol and docosahexaenoic acid (DHA; C22:6 n-3). *Steroids* 99(Pt B), 194–203. doi: 10.1016/j.steroids.2015.02.003
- Pavitt, G. D. (2018). Regulation of translation initiation factor eIF2B at the hub of the integrated stress response. *Wiley Interdiscip. Rev. RNA* doi: 10.1002/wrna.1491 [Epub ahead of print].
- Raini, G., Sharet, R., Herrero, M., Atzmon, A., Shenoy, A., Geiger, T., et al. (2017). Mutant eIF2B leads to impaired mitochondrial oxidative phosphorylation in vanishing white matter disease. *J. Neurochem.* 141, 694–707. doi: 10.1111/jnc.14024
- Ruscher, K., and Wieloch, T. (2015). The involvement of the sigma-1 receptor in neurodegeneration and neurorestoration. *J. Pharmacol. Sci.* 127, 30–35. doi: 10.1016/j.jphs.2014.11.011
- Ryskamp, D., Wu, J., Geva, M., Kusko, R., Grossman, I., Hayden, M., et al. (2017). The sigma-1 receptor mediates the beneficial effects of pridopidine in a mouse model of Huntington disease. *Neurobiol. Dis.* 97(Pt A), 46–59. doi: 10.1016/j.nbd.2016.10.006
- Sahlholm, K., Sijbesma, J. W., Maas, B., Kwizera, C., Marcellino, D., Ramakrishnan, N. K., et al. (2015). Pridopidine selectively occupies sigma-1 rather than dopamine D2 receptors at behaviorally active doses. *Psychopharmacology (Berl.)* 232, 3443–3453. doi: 10.1007/s00213-015-3997-8
- Samanta, J., Grund, E. M., Silva, H. M., Lafaille, J. J., Fishell, G., and Salzer, J. L. (2015). Inhibition of Gli1 mobilizes endogenous neural stem cells for remyelination. *Nature* 526, 448–452. doi: 10.1038/nature14957
- Schiffmann, R., and Elroy-Stein, O. (2006). Childhood ataxia with CNS hypomyelination/vanishing white matter disease—a common leukodystrophy caused by abnormal control of protein synthesis. *Mol. Genet. Metab.* 88, 7–15. doi: 10.1016/j.ymgme.2005.10.019
- Sidrauski, C., Acosta-Alvear, D., Khoutorsky, A., Vedantham, P., Hearn, B. R., Li, H., et al. (2013). Pharmacological brake-release of mRNA translation enhances cognitive memory. *Elife* 2:e00498. doi: 10.7554/eLife.00498
- Su, T. P., Su, T. C., Nakamura, Y., and Tsai, S. Y. (2016). The sigma-1 receptor as a pluripotent modulator in living systems. *Trends Pharmacol. Sci.* 37, 262–278. doi: 10.1016/j.tips.2016.01.003
- Taipale, J., Chen, J. K., Cooper, M. K., Wang, B., Mann, R. K., Milenkovic, L., et al. (2000). Effects of oncogenic mutations in smoothened and patched can be reversed by cyclopamine. *Nature* 406, 1005–1009. doi: 10.1038/35023008
- Tsaytler, P., Harding, H. P., Ron, D., and Bertolotti, A. (2011). Selective inhibition of a regulatory subunit of protein phosphatase 1 restores proteostasis. *Science* 332, 91–94. doi: 10.1126/science.1201396
- Verity, A. N., and Campagnoni, A. T. (1988). Regional expression of myelin protein genes in the developing mouse brain: in situ hybridization studies. *J. Neurosci. Res.* 21, 238–248. doi: 10.1002/jnr.490210216
- Wong, Y. L., LeBon, L., Edalji, R., Lim, H. B., Sun, C., and Sidrauski, C. (2018). The small molecule ISRIB rescues the stability and activity of Vanishing White Matter Disease eIF2B mutant complexes. *Elife* 7:e32733. doi: 10.7554/eLife.32733
- Wu, C. L., Chen, S. D., Hwang, C. S., and Yang, D. I. (2009). Sonic hedgehog mediates BDNF-induced neuroprotection against mitochondrial inhibitor 3-nitropropionic acid. *Biochem. Biophys. Res. Commun.* 385, 112–117. doi: 10.1016/j.bbrc.2009.04.145
- Wu, G., Robertson, D. H., Brooks, C. L. III, and Vieth, M. (2003). Detailed analysis of grid-based molecular docking: a case study of CDOCKER-A CHARMM-based MD docking algorithm. *J. Comput. Chem.* 24, 1549–1562. doi: 10.1002/jcc.10306
- Wyrwoll, C. S., Holmes, M. C., and Seckl, J. R. (2011). 11beta-hydroxysteroid dehydrogenases and the brain: from zero to hero, a decade of progress. *Front. Neuroendocrinol.* 32:265–286. doi: 10.1016/j.yfrne.2010.12.001
- Zhang, Y., Lv, X., Bai, Y., Zhu, X., Wu, X., Chao, J., et al. (2015). Involvement of sigma-1 receptor in astrocyte activation induced by methamphetamine via up-regulation of its own expression. *J. Neuroinflamm.* 12:29. doi: 10.1186/s12974-015-0250-7
- Zyryanova, A. F., Weis, F., Faille, A., Alard, A. A., Crespillo-Casado, A., Sekine, Y., et al. (2018). Binding of ISRIB reveals a regulatory site in the nucleotide exchange factor eIF2B. *Science* 359, 1533–1536. doi: 10.1126/science.aar5129

Conflict of Interest Statement: The authors declare that the research was conducted in the absence of any commercial or financial relationships that could be construed as a potential conflict of interest.

Copyright © 2018 Atzmon, Herrero, Sharet-Eshed, Gilad, Senderowitz and Elroy-Stein. This is an open-access article distributed under the terms of the Creative Commons Attribution License (CC BY). The use, distribution or reproduction in other forums is permitted, provided the original author(s) and the copyright owner(s) are credited and that the original publication in this journal is cited, in accordance with accepted academic practice. No use, distribution or reproduction is permitted which does not comply with these terms.